Journal of Cleaner Production 248 (2020) 119224

Contents lists available at ScienceDirect

Journal of Cleaner Production

journal homepage: www.elsevier.com/locate/jclepro

Influence of basin metals and novel wick-metal chips pad on the thermal performance of solar desalination process

Swellam W. Sharshir [a, b, c], Guilong Peng [a], Ammar H. Elsheikh [d], Mohamed A. Eltawil [e, f], M.R. Elkadeem [g], Hao Dai [a], Jianfeng Zang [b], Nuo Yang [a, *]

[a] State Key Laboratory of Coal Combustion, School of Energy and Power Engineering, Huazhong University of Science and Technology, Wuhan, 430074, China
[b] School of Optical and Electronic Information, Huazhong University of Science and Technology, Wuhan, 430074, China
[c] Mechanical Engineering Department, Faculty of Engineering, Kafrelsheikh University, Kafrelsheikh, 33516, Egypt
[d] Production Engineering and Mechanical Design Department, Faculty of Engineering, Tanta University, Tanta, Egypt
[e] Agricultural Engineering Department, Faculty of Agriculture, Kafrelsheikh University, 33516, Egypt
[f] Department of Agricultural Systems Engineering, College of Agricultural and Food Sciences, King Faisal University, P.O.Box 420 Al-Hofuf, Al-Ahsa, 31982, Saudi Arabia
[g] Electrical Power and Machines Engineering Department, Faculty of Engineering, Tanta University, Tanta, 31521, Egypt

ARTICLE INFO

Article history:
Received 28 June 2019
Received in revised form
4 November 2019
Accepted 8 November 2019
Available online 8 November 2019

Handling Editor: Jin-Kuk Kim

Keywords:
Solar desalination
Inclined wick solar still
Basin metals
Metal chips
Novel wick-metal chips pad
Thermal efficiency

ABSTRACT

In this study, efforts were made to enhance the performance of inclined wick solar still (IWSS) by integrating different basin metals and a novel wick-metal chips pad. Three different metal materials (aluminum, copper, and steel) were used as basin and their metal chips were sandwiched in a novel wick-metal pad. Experiments were carried out to figure out the influence of different basin metal materials and their metal chips filled in a wick pad on the thermal performance of IWSS. The enhanced solar still was compared with conventional inclined wick solar still (CIWSS). Results revealed that using aluminum and copper basins led to increase the productivity by 34.23% and 54.26%, respectively, compared with CIWSS. The use of metal chips sandwiched between two layers of wicks (wick-metal chips pad) caused an increase in the daily production by about 27.76%, 41.54, and 65.3% for steel, aluminum, and copper, respectively. This implies that the basin materials and the novel wick pads with metal chips, which acted as evaporation surface and heat storage medium, played a vital role in enhancing productivity. Also, the maximum thermal efficiency was 60.98% for the modified IWSS with copper basin and a novel wick-copper chips pad. While, the maximum thermal efficiency for the CIWSS with steel basin was 37%. To understand the temperature distribution through different layers of desalination surfaces, a numerical simulation was carried out under real weather conditions using the finite element software; COMSOL Multiphysics. Results showed that, there was a good agreement between experimental work and numerical investigation.

1. Introduction

Water is of major importance to human beings' survival as well as our economic activities of many sectors, such as agriculture and industry. The increase in water demand with limited resources is the most vital problem facing humanity in the recent century (Nisan and Benzarti, 2008). So, it is very essential to explore effective ways to get freshwater from alternative resources such as wastewater, brackish, ground, seawater and so on. Desalination is a promising technology to meet the global freshwater demand, because of nearly 97% of the water on the earth surface is salt water (Kalogirou, 2005). Therefore, enhancing efficiency and productivity of the solar desalination, while reducing their environmental impact in a prospective way, have been considered as major defiance and resistance of the 21st century (Shannon et al., 2008).

Desalination is an alternative solution for freshwater shortage. Removing salinity, planktons, and inclusions from a water source to get freshwater is called desalination process (Hansen et al., 2015).

* Corresponding author.
E-mail addresses: sharshir@eng.kfs.edu.eg (S.W. Sharshir), glp@hust.edu.cn (G. Peng), elsheikh@f-eng.tanta.edu.eg (A.H. Elsheikh), eltawil69@yahoo.co.in (M.A. Eltawil), mohammad.elkadim@f-eng.tanta.edu.eg (M.R. Elkadeem), dai_hao@hust.edu.cn (H. Dai), jfzang@hust.edu.cn (J. Zang), nuo@hust.edu.cn (N. Yang).

https://doi.org/10.1016/j.jclepro.2019.119224
0959-6526/

Commercially adequate, reliable and financially feasible desalination processes are based on two main methods (Khan et al., 2018); (i) membrane methods including reverse osmosis (Kim et al., 2019) and electrodialysis (Wei et al., 2020), and (ii) thermal desalination methods such as multi-stage flash (Lv et al., 2019), humidification and dehumidification (Hamed et al., 2015; Kabeel et al., 2014), multi stage flash integrated with forward osmosis (Thabit et al., 2019), multi-effect evaporation (Zhou et al., 2019), vapor compression (Chen et al., 2019). The above-mentioned desalination methods require a large amount of conventional energy (fossil fuels), have complex structures as well as form economic obstacle (Ghaffour et al., 2013). Therefore, they aren't familiar in the remote and arid regions where the water demand is not too much. Solar desalination is one type of thermal desalination technologies which uses solar energy to get potable water from non-potable water by removing impurities like high salt content, minerals, and organisms from water sources. This technique has many benefits such as zero fuel cost and eco-friendly, but it requires a large area for solar radiation collection.

Solar stills (SSs) which are usually small-scale solar desalination systems provide a solution for the shortage of water in remote and arid areas. SSs have many special features such as cheapness, can be fabricated from available local materials, and low maintenance cost (Sharshir et al., 2016c). However, SSs are not usually utilized due to higher thermal capacity and time consumption (Manikandan et al., 2013), low productivity of about 2–3 L/m^2 per day, and low thermal efficiency of about 30% (Arjunan et al., 2009). Furthermore, SSs only work during the daytime of sunrise. Therefore, there are a lot of studies have been carried out to improve and increase the productivity as well as the thermal performance of the SSs by different methods such as: nanofluids with cooling (Sharshir et al., 2017c), nano-micro particles (Sharshir et al., 2018), thin film evaporation (Elsheikh et al., 2019), nanofluid with phase change materials (Sharshir et al., 2017b), wick with heat localization (Peng et al., 2018, 2020), phase change materials (Sharshir et al., 2019b), pyramid SS (Kabeel et al., 2019), double slope SS (Fathy et al., 2018), Tubular SS (Sharshir et al., 2019a), Tubular SS with cooling (Kabeel et al., 2019). solar still with humidification and dehumidification (Sharshir et al., 2016b), and continues desalination system (Sharshir et al., 2016a).

To improve the productivity of the conventional solar still (CSS), the inclined wick solar still (IWSS), which improves the productivity by about 29.5% compared to CSS, has been proposed (Minasian and Al-Karaghouli, 1995). In IWSS, the flat basin is replaced by oblique basin which is covered with black wick materials and the water flows through the wick material and evaporates. According to (Omara et al., 2013), the IWSS has faster response and more effective than the CSS due to the large incident solar intensity absorbed by the inclined basin and result in higher operating temperatures.

Due to its high performance, IWSS has aroused a lot of interest during the past decades (Mahdi et al., 2011). studied the effect of using charcoal cloth as absorber/evaporator materials. The results concluded that charcoal cloth was a suitable material for freshwater production more than the conventional one and the increase in the input water mass flow rate led to a reduction in productivity (Hansen et al., 2015). studied the effect of different wick materials such as wood pulp paper, wicking water coral fleece fabric and polystyrene sponge on the different absorber plates (flat absorber, stepped absorber and stepped absorber with wire mesh).

(Tanaka, 2011) theoretically studied the effect of using reflectors on tilted wick solar stills. The results illustrated that productivity was improved by about 13% greater than that of IWSS (Ni et al., 2018). conducted an experimental study considering wick suspensions between the floatable insulation materials to improve the water evaporation as well as water productions; the efficiency was about 22% (Matrawy et al., 2015). studied the modified SS with corrugated basin covered by the wick and integrated with external reflectors. The results illustrated that the modified SS was improved by about 34% in the productivity compared to the CSS.

Researchers are still looking for effective ways to improve the thermal performance of solar desalination at low cost and eco-friendly behavior. Different designs of SSs have been investigated to enhance the productivity while preserving the overall cost. This can be achieved via exploiting low-cost materials with superior properties.

In the industrial process, there are metals chips produced during the machining of metals. In addition to, their disposal off is an annoying process, and recycling processes of the metal chips has also negative effect on the environment. So, this study aims to improve the performance of IWSS by utilizing different types of metals and their metal chips in the evaporation basin. In this paper, novel wick-metal chips pads were made by sandwiching metal chips between two layers of wicks. The developed wick-metal chips pad was used as a heat storage medium during daytime, a heat source during the daytime and an evaporation surface. The detailed effects of different metal basins and wick-metal chips pads on the performance were studied. Finally, the validation of the proposed system was numerically analyzed by using COMSOL Multiphysics software.

2. Experimental setup and devices

The experimental work was conducted in Kafrelsheikh city, Egypt (latitude of 31.07°N and longitude of 30.56°E) during the period from September to October 2017. Two identical inclined wick solar stills (IWSSs) were designed and manufactured as shown in Fig. 1. The IWSS has a single basin with an actual area of 0.95 m^2 (1 m length × 0.95 m width). The heights of the backside and frontside walls are 0.44 m and 0.15 m, respectively to make the top glass cover inclined with an angle of 30° with the horizontal (almost the same latitude angle of Kafrelsheikh, Egypt). At the end

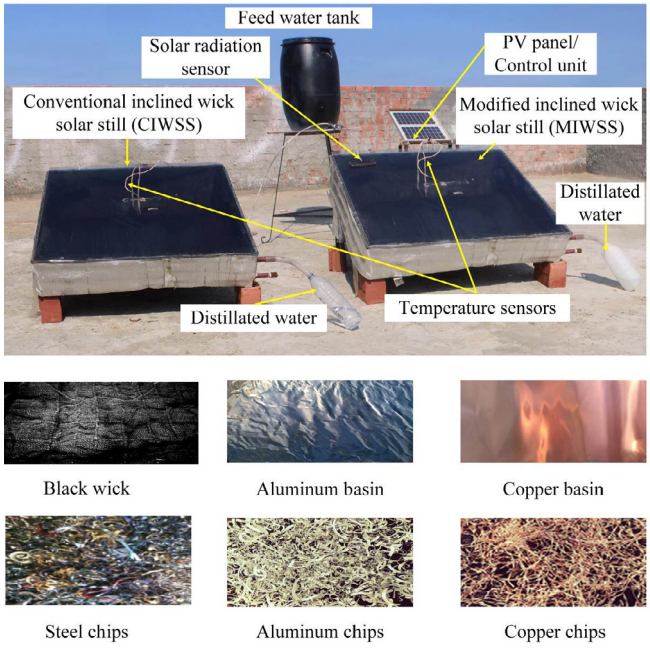

Fig. 1. Experimental setup and different components used in different modifications of IWSS.

of the backside wall, the basin was bent to form a U shape (15 cm width x 20 cm height) to collect the non-potable water and work as internal saline water tank. The basin of the solar still was inclined with an angle of 20° from the horizontal, and this is the best tilt angle according to (Omara et al., 2013). The entire basins and walls were painted from inside with black paint to maximize the absorptivity of the solar radiations. All the external walls and bottom of the basins were insulated to reduce the heat loss to the environment by using a foam sheet of 4 cm-thick which has a low thermal conductivity of about 0.038 W/m K. The clear glass cover of 4 mm thickness which has a high transmissivity of about 0.94 was used. Pipes, valves, and joints were used to control saline water flow rate from the feed tank to each IWSS. Measurements of all necessary components were assembled together as shown in Fig. 2. A small PV system (PV panel, charge controller, battery) was used to operate the control unit.

Different combinations of basin metals and novel wick pads with chips metals, which are similar to that of basin materials, were studied and compared to CIWSS. The studied combinations were steel basin covered by normal blackened wick, steel basin covered by blackened wick-steel chips pad of about 2 cm thickness, steel basin covered by aluminum basin and normal blackened wick, steel basin covered by copper basin and normal blackened wick, steel basin covered by aluminum basin and wick-aluminum chips pad of about 2 cm thickness, and a steel basin covered by copper basin and wick-copper chips pad of about 2 cm thickness. Experiments were conducted to figure out the effect of different basin metal materials as well as wick-metal chips pads on the performance of IWSS.

Ambient temperature, air velocity, and solar radiation were measured by specific digital instruments. Temperatures of the glass cover (in and out), basin, saline water in the tank, water in the still, and above the wick were measured by using LM 35 temperature sensor with an accuracy of 0.5 °C. The solar sensor was kept in the same plane of the glass cover of the IWSS and used to measure the solar radiation intensity. All measuring devices were calibrated using research lab equipment. Temperature sensors were calibrated using 590 CE calibration sensor to minimize the overall error percentage, and solar radiation sensor was calibrated by positioning it with the calibrated device (Pyranometer) at the same angle of top glass cover of IWSS. All sensors were fixed and wired to the controller unit and data were recorded on a memory card using the software in Arduino Mega (with 15 analog inputs and 53 digital I/O pins) for further analysis. Fig. 2 shows the arrangement of measuring sensors where all measured signals were transmitted through wires at specific intervals to the processing unit.

Herein, metal basin and metal chips were used to modify the IWSS as shown in Figs. 1 and 2. Steel, aluminum, and copper chips that produced during the machining operations of metals were used in the desalination unit to enhance the performance of the IWSS. These chips were sandwiched between two layers of wick materials to form a novel wick-metal chips pad and to enhance the water productivity as well as the thermal performance.

2.1. Experimental procedure

The performance of modified inclined wick solar still (MIWSS) was investigated by using different combinations of basin metals such as steel, aluminum, and copper as well as novel wick-metal chips pads. Different properties of metals used in this work are presented in Table 1. It should mention that the dry bulk density of

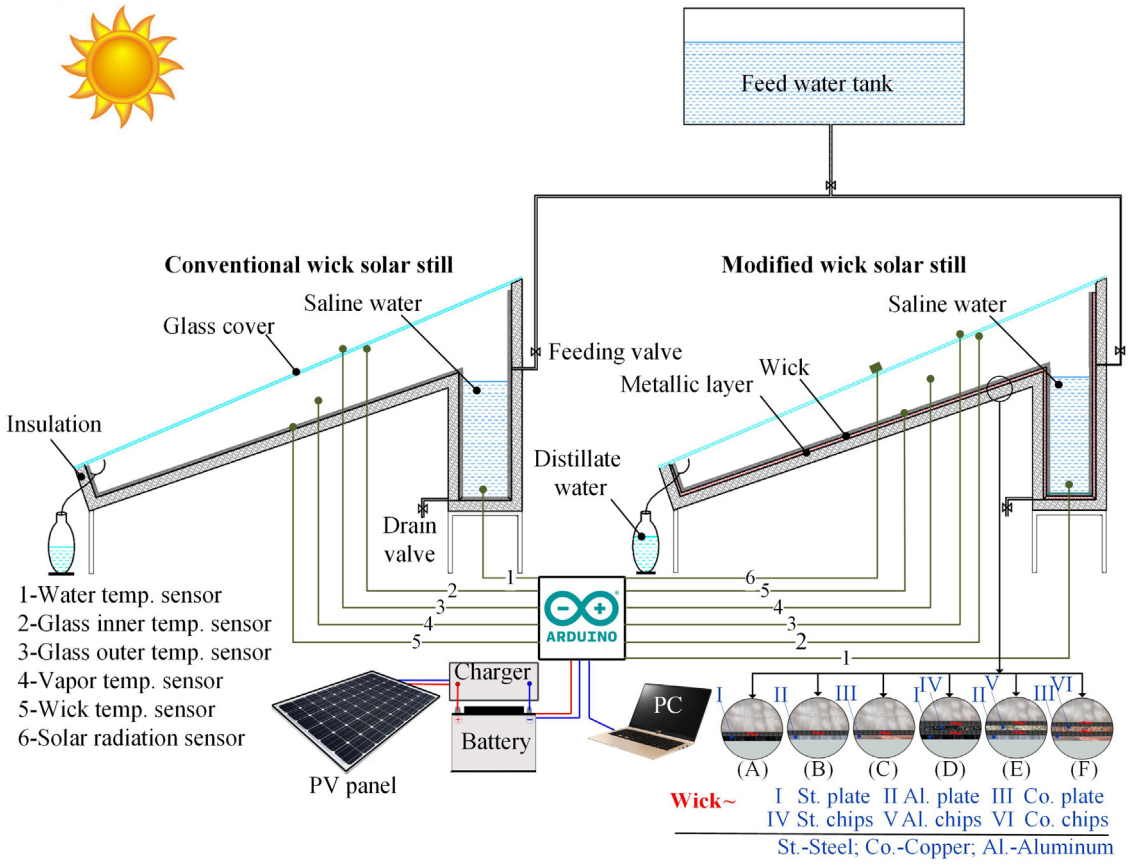

Fig. 2. Schematic diagram of the desalination setup and data acquisition system.

the metal chips is 357, 306, and 408 kg/m^3 for steel, Al, and Cu, respectively. While, the wet bulk density of the novel wick-metal chips pads is 433.67, 382.65, and 459.18 kg/m^3 for steel, Al and Cu, respectively.

Furthermore, the basin and chips metals were painted by black paint to increase the absorptivity of solar radiation, hence identifying which basin/chips give the best performance. The wick-metal chips pad that used in MIWSS basin acted as a surface of evaporation. The water flow through the wick pad due to the capillary action, which served as a thin layer of water, therefore improved the evaporation rate. The water vapor was condensed on the inner surface of glass cover due to the temperature difference and collected again to determine the productivity.

The experiments were conducted in six configurations to investigate the effect of basin metals and wick-metal chips pads on the productivity and thermal performance of IWSS. The used two stills basins were made from 1.5 mm steel, then the basin of one still was covered by two layers of blackened wick without any modifications (CIWSS or control), while the other solar still was modified through some additions. The MIWSS was modified by covering the steel basin with either aluminum basin or copper basin. Above the second added basin there was a novel wick-metal chips pad. To fulfill the function of a novel wick pad, there were some changes made to the pad by using two layers of the normal blackened wick, sandwiching one metal chips either steel, aluminum or copper between the two layers of wicks. The experimental tests were carried out in several stages given in Table 2.

2.2. Mathematical modelling

To figure out the effect of using different configurations of metals in the multilayer basin, wick-metal chips pad, and insulations, the well-known finite element software COMSOL Multiphysics has been used to accurate modeling of the proposed systems and obtain the temperature distribution through different layers considering real-weather conditions. The following heat transfer coefficients and relations were used in the numerical simulation:

2.2.1. Convective heat transfer

The convection heat transfer coefficient ($h_{C,w-g}$) between the wick surface and the adjacent air layer is defined as (Velmurugan et al., 2008):

$$h_{C,w-g} = 0.884\left\{(T_w - T_g) + \frac{[P_w - P_g][T_w]}{[268900 - p_w]}\right\}^{1/3} \quad (1)$$

where, P_w and P_g are the partial pressure of humidified air at the water surface and the inner surface of the glass cover, respectively, which are given by (Sharshir et al., 2017a):

$$P_w = \exp\left[25.317 - \frac{5144}{T_w}\right] \quad (2)$$

$$P_g = \exp\left[25.317 - \frac{5144}{T_g}\right] \quad (3)$$

2.2.2. Radiative heat transfer (RHT)

The radiative heat transfer coefficient ($h_{R,w-g}$) between the glass inner surface and wick surface directly without physical medium is defined by (Velmurugan et al., 2008):

$$h_{R,w-g} = \varepsilon_{eff}\sigma\left[(T_w + 273)^2 + (T_g + 273)^2\right](T_w + T_g + 546) \quad (4)$$

where σ is Stefan-Boltzmann constant and ε_{eff} is the effective emissivity between the wick and the inner glass surfaces and is given by:

$$\varepsilon_{eff} = \left(\frac{1}{\varepsilon_w} + \frac{1}{\varepsilon_g} - 1\right)^{-1} \quad (5)$$

2.2.3. Evaporative heat transfer

The evaporative heat transfer coefficient ($h_{E,w-g}$) is one of the most important mechanisms of heat transfer inside the solar still which means evaporations of water from the wick to the bulk air in the still and is given by (Velmurugan et al., 2008):

$$h_{E,w-g} = 16.273 \times 10^{-3} \times h_{C,w-g} \times \left[\frac{P_w - P_g}{T_w - T_g}\right] \quad (6)$$

The outer convective heat transfer (h_{b-a}) between the basin and ambient air is a relation in wind velocity (V) and is given by:

$$h_{b-a} = 2.5 + (3 \times V) \quad (7)$$

The overall heat transferred from the wick surface is the summation of heat transferred via the aforementioned mechanisms (convective, radiative and evaporative).

The numerical simulation using COMSOL Multiphysics on the heat transfer coefficients and relations on type A, type B, and type C was verified using the real experimental results.

2.3. System thermal performance

To assess the thermal performance of the studied wick SSs, the thermal energy efficiency was determined under real operating conditions (Sharshir et al., 2017a).

The daily thermal energy efficiency,η is given by

Table 1
Properties of different materials used in the experimental setup.

Materials	Thermal conductivity W/(m. K)	Density, kg/m^3	Specific heat, J/(kg. K)	Thermal diffusivity, m^2/s
Steel	44.5	7850	475	1.19 x 10^{-5}
Al	200	2700	900	8.23 x 10^{-5}
Cu	401	8960	385	11.62 x 10^{-5}
Wick	0.089	1000	4187	2.12 x 10^{-8}
Glass	0.96	2700	84	3.4 × 10^{-7}
Insulation	0.031	55	1800	3.13 x 10^{-7}

Table 2
The detailed description and components of each stage.

Stage	Procedure of each type
Type A	Type A (Steel + two layers of blackened wick) was used as a reference configuration
Type B	Type B (Steel + Al + two layers of blackened wick) was compared with type A
Type C	Type C (Steel + Cu + two layers of blackened wick) was compared with type A
Type D	Type D (Steel + Steel chips sandwiched between two layers of blackened wick) was compared with type A
Type E	Type E (Steel + Al + Al chips sandwiched between two layers of blackened wick) was compared with type A
Type F	Type F (Steel + Cu + Cu chips sandwiched between two layers of blackened wick) was compared with type A

$$\eta = \frac{\sum m_{ew} \times h_{fg}}{\sum I(t) \times A_s \times 3600} \quad (8)$$

where, $m_{ew}$is the hourly distillate water, h_{fg} is the water evaporative latent heat which equals to 2335 kJ/kg, $I(t)$is the hourly solar radiation and $A_s$is the surface area of the wick [24, 25]. Results of the present study were compared with the previous investigators in terms of productivity and thermal efficiency.

3. Results and discussions

3.1. Effect of using different metals in the basin of MIWSS

Experiments were carried out on several sunny days during the period from September to October 2017. Weather data revealed that the ambient air temperature was varied from about 26 °C to 36 °C, the insolation was varied from 0 W /m^2 to about 1000 W/m^2 at noon, and the wind speed was varied from 1.3 m/s to 5.1 m/s. Fig. 3 (a) shows the variation of solar radiation and ambient temperature with respect to the daytime during two sunny days. It is clear that the solar intensity and the surrounding air temperature had a narrow variation and followed the same trend.

Several tests were performed covering various modifications and operating conditions to record the temperature of different components. Fig. 3 (b) and 3 (c) illustrates the variation of wick and glass temperatures during the daytime for the first three modifications mentioned in Table 2. It is clear that the highest wick and glass temperatures were recorded with the basin of type C followed by basins of type B and A. The wick and glass temperatures increased from their lower values in the morning to the peak values at 1:00 p.m. due to the increase in solar radiation and ambient temperature.

Also, Fig. 3-(b) illustrates the wick temperatures for types A, B, and C. We can observe that the wick temperature increased from the morning to the maximum value at 1:00 p.m. for the three types due to increasing the solar radiation and ambient temperature. Also, the temperature of wick materials with copper and aluminum basin, were larger than that with steel basin by about 3.3–14.3 °C for copper basin and 1 to 8.2 °C for aluminum basin due to the higher thermal conductivity of copper and aluminum than that of the steel as mentioned before where the maximum value of wick with copper basin was about 78.95 °C and with aluminum basin was about 75 °C but for wick with steel basin was 67.7 °C at 1:00 p.m. Increasing the thermal conductivity increases the heat absorption as well as heat loss to the wet wick and the water in the solar still.

On the other hand, the difference in glass temperature between type B and type A was about 0.27 °C at 6:00 p.m. and 3 °C at 11:00a.m. as shown in Fig. 3- (c), and the glass temperature difference between types A and C was about 0.88 °C at 6:00 p.m. and 4.4 °C at 1:00 p.m. It is obvious that the difference in glass temperature between types A, B, and C were less than the difference in wick temperature which indicates that the temperature difference between the glass and wick for type C was higher than type B. Finally, type A has the lowest value of temperature difference between the glass and the wick during the daytime which means that the productivity of type C was always higher than types B, and A and productivity of type B was always higher than type A as illustrated in Fig. 3-(d).

Furthermore, the hourly and daily alteration of water production for types A, B, and C are shown in Fig. 3- (d) and (c) within the time from 8:00 a.m. to 6.00 p:m. Fig. 3- (d) illustrated the hourly productivity for the three types of IWSS. Results revealed that the distillate production during the daytime for the type A was smaller than that of types B and C. This is basically due to the temperatures of the wick in types C and B during the daytime were higher than that in type A as illustrated in Fig. 3- (b). Also, Fig. 3- (d) illustrates the maximum hourly productivity which was 0.815 L/m^2, 0.99 L/m^2, and 1.1 L/m^2 for types A, B, and C respectively, at 1:00 p.m. Furthermore, the total productivity of types B and C was improved by approximately 34.23% and 54.26% compared with type A during the daytime from 8:00 a.m. to 6:00 p.m. The increase in the temperature and productivity may be due to the increase in thermal conductivity (heat transfer) between the basin and wick. Also, the aluminum and copper metals of the basin worked as a sensible heat source. Hence, the system temperature and evaporation rate as well as productivity were increased.

3.2. Effects of metal chips on the MIWSS performance

The distribution of ambient temperature and solar irradiance for three different testing days is plotted in Fig. 4-(a). It can be observed that the climatic conditions have trivial change during the different testing days. The temperature difference between the wick and the inner surface of the glass cover for different types of MIWSS is shown in Fig. 4-(b).

With high thermal conductivity and large surface area, the metals chips worked as an energy storage as well as a source of heat during the daytime. The heat source and energy storage start from the morning with sun rise. They can heat up quickly because they are in thin layer and has good thermal conductivity. Moreover, it loses the heat to wick martials quickly which increase the freshwater production. Both heat source and energy storage increase from the morning to the afternoon at 2:00 p.m., as a result of increasing the maximum temperature difference between the glass and the wick was observed at 2:00 p.m. After that, temperature difference between the glass and the wick started to decrease till the minimum value at the end of the experiment at 6:00 p.m. as illustrated in Fig. 4 – (b). This also because of the metal chips cannot catch the stored energy for a long time (i.e. during the nighttime).

The given results revealed that the temperature difference between the wick and the inner surface of the glass cover of the MIWSSs with a novel wick-metal chips pad was increased compared with CIWSS. From Fig. 4- (b), the highest wick/glass temperature difference was recorded for basin type F followed by basin types E, D, and A, respectively. Notably, the peaks value of the

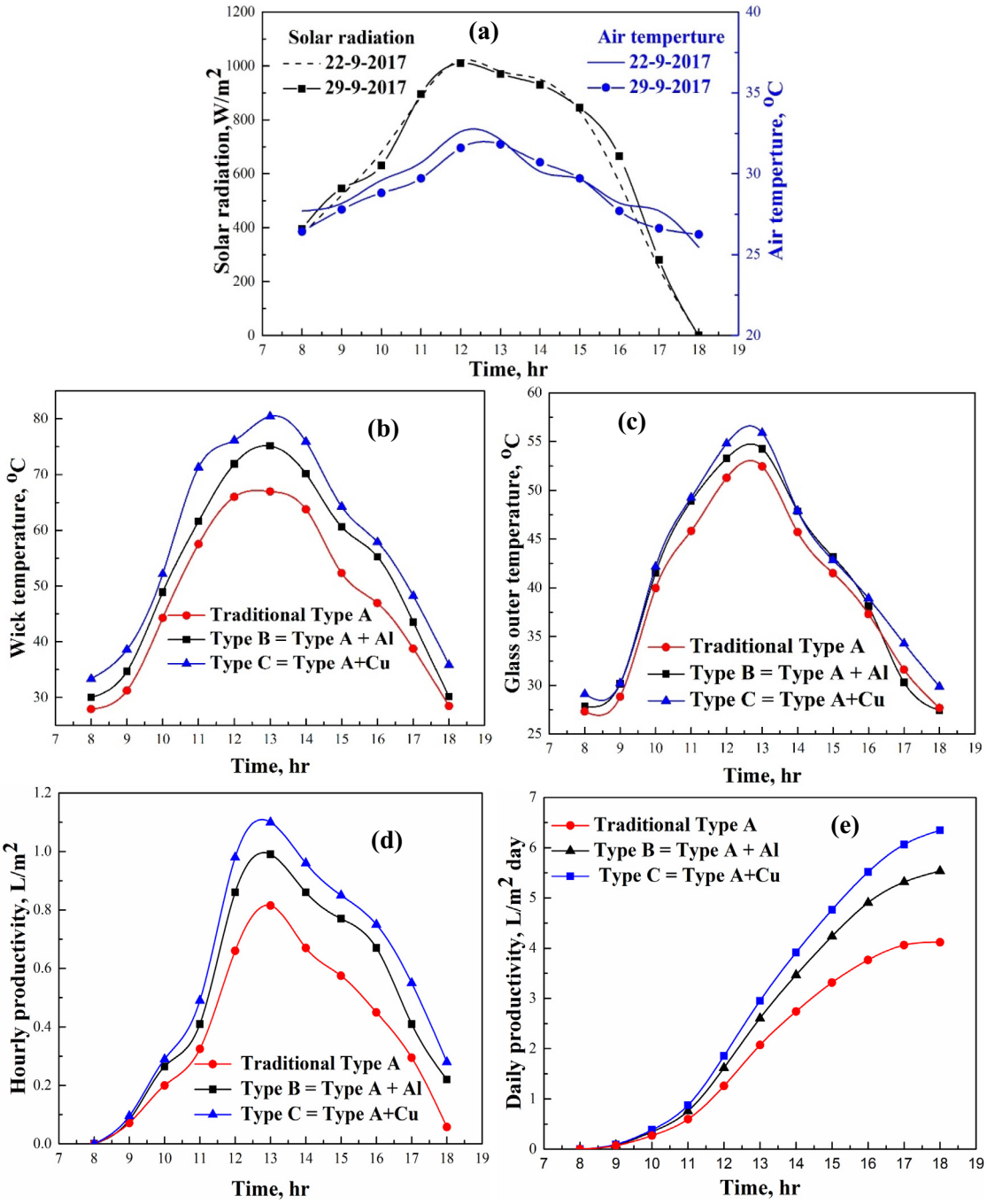

Fig. 3. Change over time (a) Hourly air temperature and solar radiation, (b) Wick temperature, (c) Hourly glass temperatures, (d) Hourly water production, (e) Daily water production. Where type A "steel + two layers of wick", type B "Steel + Al + two layers of wick" and type C "Steel + Cu + two layers of wick".

highest temperature difference for all types occurs at 2:00 p.m. This mainly attributed to the increase in the solar radiation and ambient temperature from the morning to the noon. The wick/glass temperature difference increased from lower value in the morning to the peak value at noon (1:00 p.m.). The temperature difference was increased from 1.11 to 8 °C, from 2 to 20 °C, from 3.5 to 24 °C, and from 6.5 to 32 °C for types A, D, E and F respectively, and after 1:00 p.m. the temperature difference started to decrease as illustrated in Fig. 4-(b). In addition to the high wick/glass temperature difference in case of using wick-metal chips pad over the conventional still which resulted in enhancing the condensation rate; the use of metal chips increased the evaporation surface area, and consequently improved the evaporation rate compared to the conventional one.

For comprehensive assessment of the performance of the proposed systems, the hourly output yield for MIWSSs with types D, E, and F compared to the CIWSS (type A) during the time from 8:00 a.m. to 6:00 p.m. is shown in Fig. 5 (a), (b) and (c), respectively. This figure shows that the hourly output yield for the all MIWSSs was constantly higher than that of type A.

Moreover, the results illustrated that the increase in chips temperature increased the yield for the MIWSS with steel basin/chips (type D), aluminum basin/chips (type E), and copper basin/chips (type F). Fig. 5- (a), (b) and (c) demonstrated that the hourly

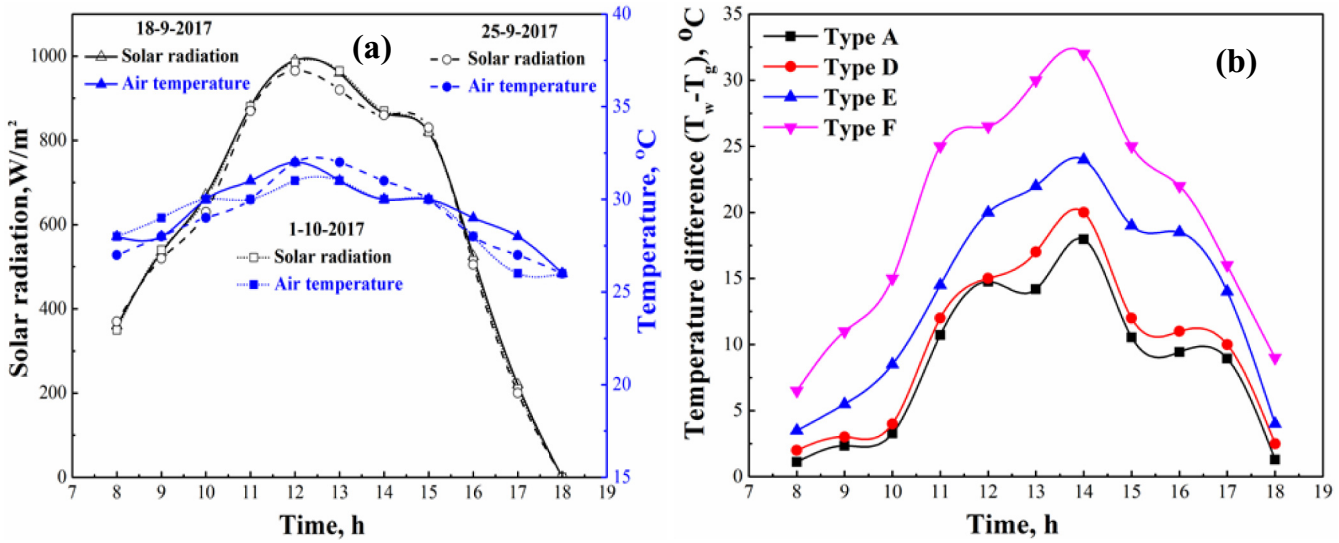

Fig. 4. (a) Hourly air temperature and global solar radiation for different days during experiments; (b) Average temperature differences between wick and glass: where type A steel + two layers of wick, type D = type A + steel chips pad, type E = type A + Al + Al chips pad and type F = type A + Cu + Cu chips pad.

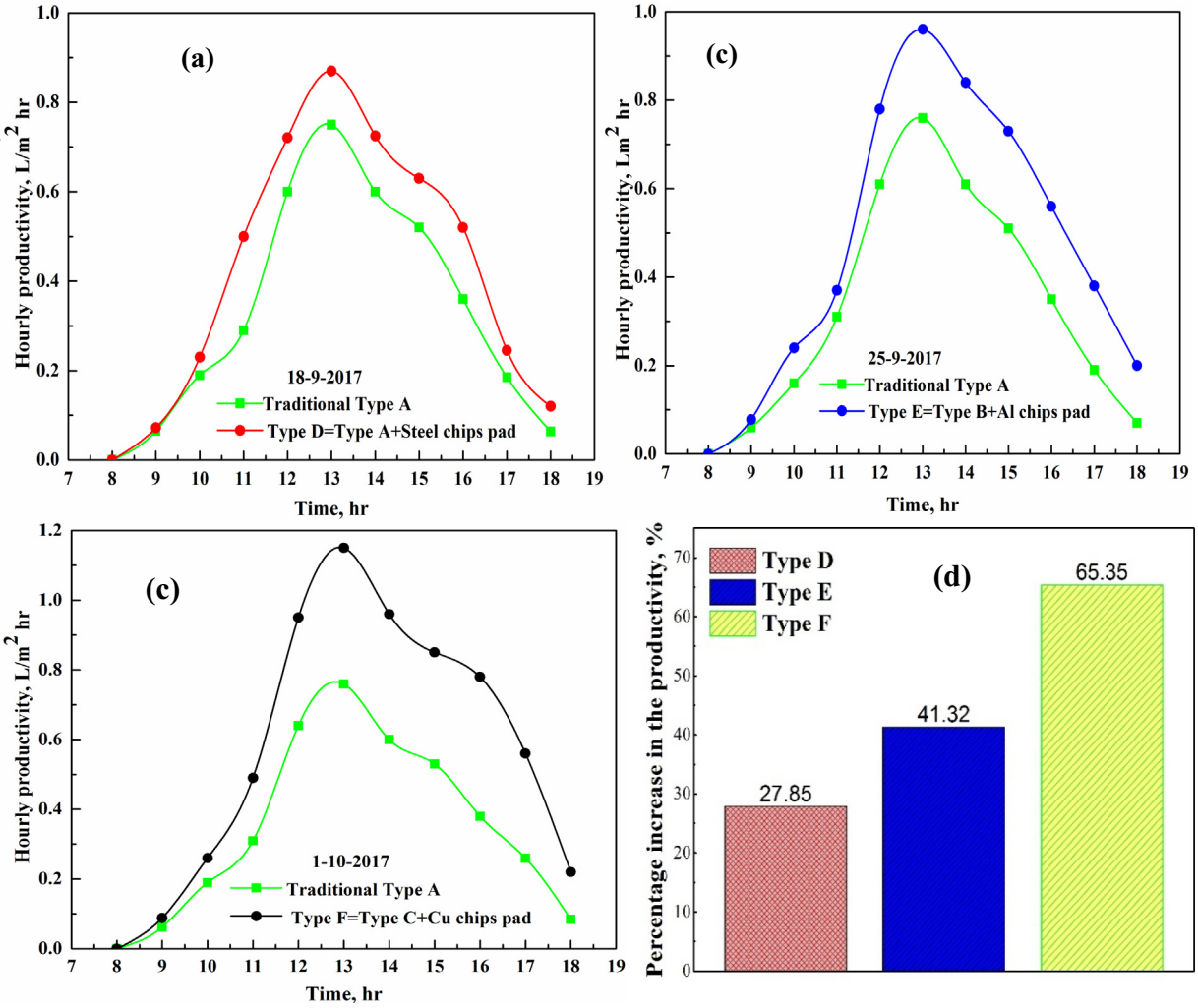

Fig. 5. Change productivity over time (a) hourly water production of types D & A; (b) hourly water production of type E & A, (c) hourly water production of types F & and A, (d) percentage increase in the productivity. Where type D = type A + steel chips pad, type E = type B + Al chips pad and type F = type C + Cu chips pad.

yield for the MIWSSs was larger than that of CIWSS during the day due to the increase of temperature of wick-metal chips, thus the evaporation rate.

As shown in Fig. 5- (a), during the experimental day of 18-09-2017, the output yield for types D and A was about 0.0 at 8:00 a.m., thereafter the output yield increased and reached up to 0.92 L/(m^2.h) and 0.81 L/(m^2.h), respectively at 1:00 p.m. Fig. 5- (b) illustrates the output yield for type E compared to type A during the experimental day of 25-09-2017, where it was about 0.0 at 8:00 a.m., and after that the yield increased to 0.96 L/(m^2.h) and 0.76 L/(m^2.h), respectively at 1:00 p.m. Fig. 5- (c) shows the productivity of type F compared to type A on 01-10-2017, which was about 0.0 at 8:00 a.m., then increased to around 1.15 L/(m^2.h) and 0.76 L/(m^2.h), respectively at 1:00 p.m.

The mean results illustrated that the accumulated output yield of type D with steel and type A reached up to around 5.28 L/(m^2.day) and 4.13 L/(m^2.day), respectively. The increase in accumulated freshwater productivity for type D was 27.84% larger than that of type A as presented in Fig. 5- (d). Furthermore, the accumulated output yield of types E and A reached up to 5.13 L/(m^2.h) and 3.63 L/(m^2.h), respectively. The increase in accumulated freshwater productivity for type E was about 41.32% larger than the type A as given in Fig. 5- (d). Finally, the accumulated output yield of types F and A reached up to 6.30 L/(m^2.h) and 3.81 L/(m^2.h), respectively. The increase in accumulated freshwater productivity for type F was 65.3% larger than type A as illustrated in Fig. 5-(d).

4. System validation

For proper evaluation of the proposed MIWSSs, a numerical simulation was carried out under real weather conditions using the finite element software; COMSOL Multiphysics. Fig. 6 shows the temperature distributions in different layers in selected three types-A, B and C (type A = steel + wick, type B = steel + Al + wick, and type C = steel + Cu + wick) in addition to the insulation for all types. It was noticed that there were no temperature differences between different layers in the three studied types at the beginning of the day (at 8:00 a.m.) as illustrated in the Fig. 6. With the increase

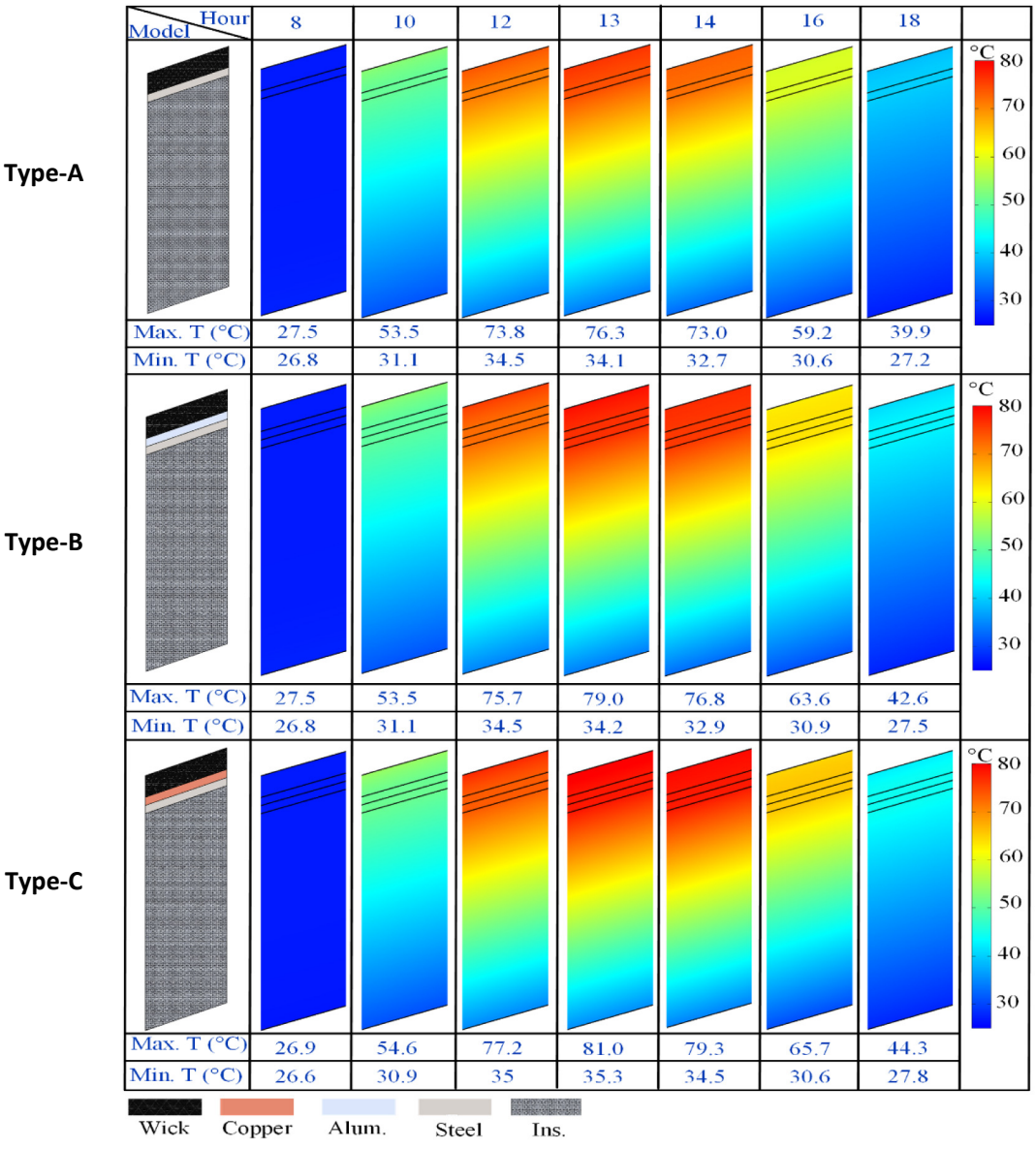

Fig. 6. Temperature distributions during the daytime in different layers for types A, B and C which obtained from the numerical simulation.

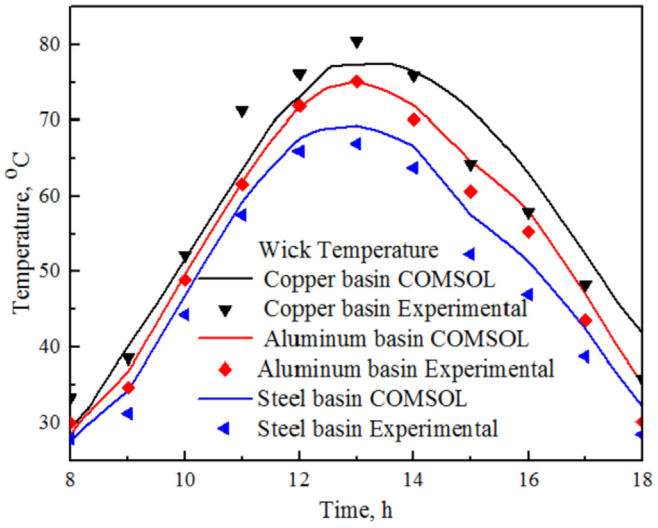

Fig. 7. Validation of the numerical simulation with the experimental data for the three types A, B and C of the IWSS.

in solar radiation, the temperature increased in the different layers for all types at 10:00 a.m. Also, it was clear that the higher temperature occurred in the wick flowed by metal. Furthermore, the lowest temperature was found in the thermal insulations; as the range of temperature inside the thermal insulations formed the highest temperature value adjacent to the metal while the lowest temperature value, was almost similar to the temperature of the surrounding air. However, the maximum temperature of the system was obtained at 1:00 p.m. which was in the wick and metals as shown in all types. The maximum temperatures achieved at 1:00 p.m. were 76.3 °C, 79 °C and 81 °C for type A (steel + wick), type B (steel + Al + wick) and type C (steel + Cu + wick), respectively as shown in Fig. 6.

Fig. 7 shows the comparison between the numerical simulation and experimental data for the three types of IWSSs. Obviously, there was a good agreement between the numerical simulation and experimental data for the wick temperatures. The average wick temperature in steel case from numerical simulation and experimental work was about 52.37 °C and 47.63 °C, respectively which revealed an increase of about 9.9%. While, in the aluminum basin, the average wick temperature in the aluminum case from numerical simulation and experimental work was about 56.74 °C and 52.88 °C, respectively which indicated an increase of about 7.25%. Furthermore, in the steel basin, the average wick temperature in the steel case from numerical simulation was about 60.38 °C but from the experimental was about 57.74 °C which increased by about 4.74%. This difference may be due to surrounding conditions that are considered constant with time, in numerical simulation, while they change with time during the experiments.

5. System thermal performance

Table 3 illustrates the accumulated output productivity and daily thermal energy efficiency for the MIWSS and CIWSS. Six types A, B, C, D, E, and F where (type A = steel + wick, type B = steel + Al + wick, type D = type A + steel chips pad, type E = type B + Al chips pad and type F = type C + Cu chips pad. Each type has been experimented for three days and the average results are presented in Table 3. Moreover, the comparison between the present results and previous relevant studies are presented in Table 4.

6. Conclusions

In this work, different basin materials (i.e., different absorber

Table 3
Comparison between daily output yield and thermal energy efficiency for different types of IWSS.

Date	Modifications made in the basin	Total yield L/(m^2 day)	Increase in productivity, (%)	Thermal efficiency, (%)
20/09/2017	Type A	4.15	34.93	37.9
	Type B	5.60		51.15
22/09/2017	Type A	4.12	34.22	37.04
	Type B	5.53		49.72
23/09/2017	Type A	4.1	33.65	36.9
	Type B	5.48		49.36
26/09/2017	Type A	4.09	56.47	37.1
	Type C	6.4		58
29/09/2017	Type A	4.11	54.26	36.67
	Type C	6.34		56.57
28/09/2017	Type A	4.0	54	36.2
	Type C	6.16		55.78
16/09/2017	Type A	4	28.75	37
	Type D	5.15		47.7
18/09/2017	Type A	4.13	27.84	36.79
	Type D	5.28		46.12
19/09/2017	Type A	4.1	26.82	36.4
	Type D	5.2		46.2
24/09/2017	Type A	3.65	41.91	35.3
	Type E	5.18		50.14
25/09/2017	Type A	3.63	41.32	35.14
	Type E	5.13		50.5
26/09/2017	Type A	3.6	38.88	35.1
	Type E	5		48.76
30/09/2017	Type A	3.83	65.7	37.07
	Type F	6.35		61.47
01/10/2017	Type A	3.81	65.35	36.8
	Type F	6.30		60.98
03/10/2017	Type A	3.75	65.3	36.03
	Type F	6.2		59.6

Table 4
Comparison between the present study and previous relevant studies

Reference	Modifications	Productivity L/ (m^2.day)	Efficiency, %
Present work	Copper basin and a novel wick pad copper chip	6.3	60.9
	Aluminum basin and a novel wick pad aluminum chip	5.13	50.5
	Steel basin and a novel wick pad steel chip	5.28	46.12
	Copper basin with double layer wick	6.34	56.5
	Aluminum basin with double layer wick	5.13	49.7
	Steel basin with double layer wick (reference)	4.12	36
(Kabeel, 2009)	Concave shaped wick surface	4.1	30
(Alaian et al., 2016)	Pin-finned basin with wick materials	4.87	55
(Tanaka and Iishi, 2017)	Horizontal multiple- impact diffusion integrated with a tilted wick	4.88	55
(Ni et al., 2018)	Wick suspensions between the floatable insulation materials	2.5	22

plates) such as steel (type A), aluminum (type B), and copper (type C) were proposed. Also, the perfromace of different developed configurations of basins and novel wick-metal chips pads, such as type D (steel basin + wick-steel chips pad), type E (aluminum basin + wick-aluminum chips pad), and type F (copper basin + wick-copper chips pad) in MIWSS were investigated. Based on this study, type F was found to be the best one which gave the highest performance, in terms of thermal efficiency and productivity. Furthermore, the finite element software COMSOL Multiphysics has been used to obtain the temperature distribution through different layers considering real-weather conditions, in which a good agreement between experimental and numerical simulation results have been obtained.

The main results are summarized in the following:

- The daily production of types B, C, and A was 5.53 L/m^2, 6.35 L/m^2, and 4.11 L/m^2, respectively.
- Using types B and C in the MIWSS improved the water production by about 34.23% and 54.26%, respectively, compared with type A.
- Using types E and F in the MIWSS enhanced the water production by about 41.39% and 65.3%, respectively compared with type A.
- Daily efficiencies were about 49.72%, 56.57%, 46.12%, 50.5%, and 60.98% which corresponding to types B, C, D, E, and F, respectively. Furthermore, the daily efficiency of the type A ranged between 35 and 37%.
- The deviations between experimental and numerical simulation results were only 9.9%, 7.25% and 4.74% for types A, B, and C, respectively.

Declaration of competing interest

The authors declare that they have no known competing financial interests or personal relationships that could have appeared to influence the work reported in this paper.

Acknowledgments

The work was sponsored by National Natural Science Foundation of China No. 51950410592 (S.W.S.) and No. 51576076 (N.Y.) and Fundamental Research Funds for the Central Universities (2019kfyRCPY045). The authors thank the National Supercomputing Center in Tianjin (NSCC-TJ) and China Scientific Computing Grid (ScGrid) for providing assistance in computations.

Nomenclatures

$h_{C,w-g}$	Convection heat transfer coefficient
$h_{R,w-g}$	Radiative heat transfer coefficient
$h_{E,w-g}$	Evaporative heat transfer coefficient
h_{b-a}	Convective heat transfer between the basin and ambient
h_{fg}	Water evaporative latent heat
P	Partial pressure
T	Temperature

Abbreviations

A	Area
IWSS	Inclined wick solar still
CIWSS	Conventional inclined wick solar still
MIWSS	modified inclined wick solar still
SSs	Solar stills
CSS	Conventional solar still
Al	Aluminum plate
Cu	Copper plate
V	Wind velocity
m_{ew}	Hourly distillate

Greek letters

η	Daily efficiency
σ	Stefan-Boltzmann constant
ε_{eff}	Effective emissivity

Subscripts

g	Glass
w	Water
s	Surface area of the wick

References

Alaian, W.M., Elnegiry, E.A., Hamed, A.M., 2016. Experimental investigation on the performance of solar still augmented with pin-finned wick. Desalination 379, 10–15.
Arjunan, T.V., Aybar, H.Ş., Nedunchezhian, N., 2009. Status of solar desalination in India. Renew. Sustain. Energy Rev. 13 (9), 2408–2418.
Chen, Q., Ja, M.K., Li, Y., Chua, K.J., 2019. Energy, exergy and economic analysis of a hybrid spray-assisted low-temperature desalination/thermal vapor compression system. Energy 166, 871–885.
Elsheikh, A.H., Sharshir, S.W., Ahmed Ali, M.K., Shaibo, J., Edreis, E.M.A., Abdelhamid, T., Du, C., Haiou, Z., 2019. Thin film technology for solar steam generation: a new dawn. Sol. Energy 177, 561–575.
Fathy, M., Hassan, H., Salem Ahmed, M., 2018. Experimental study on the effect of coupling parabolic trough collector with double slope solar still on its performance. Sol. Energy 163, 54–61.
Ghaffour, N., Missimer, T.M., Amy, G.L., 2013. Technical review and evaluation of the economics of water desalination: current and future challenges for better water supply sustainability. Desalination 309, 197–207.
Hamed, M.H., Kabeel, A.E., Omara, Z.M., Sharshir, S.W., 2015. Mathematical and experimental investigation of a solar humidification–dehumidification desalination unit. Desalination 358, 9–17.
Hansen, R.S., Narayanan, C.S., Murugavel, K.K., 2015. Performance analysis on inclined solar still with different new wick materials and wire mesh. Desalination 358, 1–8.
Kabeel, A.E., 2009. Performance of solar still with a concave wick evaporation surface. Energy 34 (10), 1504–1509.
Kabeel, A.E., Hamed, M.H., Omara, Z.M., Sharshir, S.W., 2014. Experimental study of a humidification-dehumidification solar technique by natural and forced air

circulation. Energy 68, 218–228.
Kabeel, A.E., Sharshir, S.W., Abdelaziz, G.B., Halim, M.A., Swidan, A., 2019. Improving performance of tubular solar still by controlling the water depth and cover cooling. J. Clean. Prod. 233, 848–856.
Kalogirou, S.A., 2005. Seawater desalination using renewable energy sources. Prog. Energy Combust. Sci. 31 (3), 242–281.
Khan, M.A.M., Rehman, S., Al-Sulaiman, F.A., 2018. A hybrid renewable energy system as a potential energy source for water desalination using reverse osmosis: a review. Renew. Sustain. Energy Rev. 97, 456–477.
Kim, J., Park, K., Yang, D.R., Hong, S., 2019. A comprehensive review of energy consumption of seawater reverse osmosis desalination plants. Appl. Energy 254, 113652.
Lv, H., Wang, Y., Wu, L., Hu, Y., 2019. Numerical simulation and optimization of the flash chamber for multi-stage flash seawater desalination. Desalination 465, 69–78.
Mahdi, J.T., Smith, B.E., Sharif, A.O., 2011. An experimental wick-type solar still system: design and construction. Desalination 267 (2), 233–238.
Manikandan, V., Shanmugasundaram, K., Shanmugan, S., Janarthanan, B., Chandrasekaran, J., 2013. Wick type solar stills: a review. Renew. Sustain. Energy Rev. 20, 322–335.
Matrawy, K.K., Alosaimy, A.S., Mahrous, A.F., 2015. Modeling and experimental study of a corrugated wick type solar still: comparative study with a simple basin type. Energy Convers. Manag. 105, 1261–1268.
Minasian, A.N., Al-Karaghouli, A.A., 1995. An improved solar still: the wick-basin type. Energy Convers. Manag. 36 (3), 213–217.
Ni, G., Zandavi, S.H., Javid, S.M., Boriskina, S.V., Cooper, T.A., Chen, G., 2018. A salt-rejecting floating solar still for low-cost desalination. Energy Environ. Sci. 11 (6), 1510–1519.
Nisan, S., Benzarti, N., 2008. A comprehensive economic evaluation of integrated desalination systems using fossil fuelled and nuclear energies and including their environmental costs. Desalination 229 (1), 125–146.
Omara, Z.M., Eltawil, M.A., ElNashar, E.A., 2013. A new hybrid desalination system using wicks/solar still and evacuated solar water heater. Desalination 325, 56–64.
Peng, G., Deng, S., Sharshir, S.W., Ma, D., Kabeel, A.E., Yang, N., 2020. High efficient solar evaporation by airing multifunctional textile. Int. J. Heat Mass Transf. 147, 118866.
Peng, G., Ding, H., Sharshir, S.W., Li, X., Liu, H., Ma, D., Wu, L., Zang, J., Liu, H., Yu, W., Xie, H., Yang, N., 2018. Low-cost high-efficiency solar steam generator by combining thin film evaporation and heat localization: both experimental and theoretical study. Appl. Therm. Eng. 143, 1079–1084.
Shannon, M.A., Bohn, P.W., Elimelech, M., Georgiadis, J.G., Mariñas, B.J., Mayes, A.M., 2008. Science and technology for water purification in the coming decades. Nature 452, 301.
Sharshir, S.W., Ellakany, Y.M., Algazzar, A.M., Elsheikh, A.H., Elkadeem, M.R., Edreis, E.M.A., Waly, A.S., Sathyamurthy, R., Panchal, H., Elashry, M.S., 2019a. A mini review of techniques used to improve the tubular solar still performance for solar water desalination. Process Saf. Environ. Prot. 124, 204–212.
Sharshir, S.W., Elsheikh, A., Edreis, E.M.A., Ahmed Ali, M., Sathyamurthy, R., Kabeel, A.E., Zang, J., Yang, N., 2019b. Improving the solar still performance by using thermal energy storage materials: a review of recent developments. Desalin. Water.Treat 165, 1–15.
Sharshir, S.W., Elsheikh, A.H., Peng, G., Yang, N., El-Samadony, M.O.A., Kabeel, A.E., 2017a. Thermal performance and exergy analysis of solar stills – a review. Renew. Sustain. Energy Rev. 73, 521–544.
Sharshir, S.W., Peng, G., Elsheikh, A.H., Edreis, E.M.A., Eltawil, M.A., Abdelhamid, T., Kabeel, A.E., Zang, J., Yang, N., 2018. Energy and exergy analysis of solar stills with micro/nano particles: a comparative study. Energy Convers. Manag. 177, 363–375.
Sharshir, S.W., Peng, G., Wu, L., Essa, F.A., Kabeel, A.E., Yang, N., 2017b. The effects of flake graphite nanoparticles, phase change material, and film cooling on the solar still performance. Appl. Energy 191, 358–366.
Sharshir, S.W., Peng, G., Wu, L., Yang, N., Essa, F.A., Elsheikh, A.H., Mohamed, S.I.T., Kabeel, A.E., 2017c. Enhancing the solar still performance using nanofluids and glass cover cooling: experimental study. Appl. Therm. Eng. 113, 684–693.
Sharshir, S.W., Peng, G., Yang, N., El-Samadony, M.O.A., Kabeel, A.E., 2016a. A continuous desalination system using humidification – dehumidification and a solar still with an evacuated solar water heater. Appl. Therm. Eng. 104, 734–742.
Sharshir, S.W., Peng, G., Yang, N., Eltawil, M.A., Ali, M.K.A., Kabeel, A.E., 2016b. A hybrid desalination system using humidification-dehumidification and solar stills integrated with evacuated solar water heater. Energy Convers. Manag. 124, 287–296.
Sharshir, S.W., Yang, N., Peng, G., Kabeel, A.E., 2016c. Factors affecting solar stills productivity and improvement techniques: a detailed review. Appl. Therm. Eng. 100, 267–284.
Tanaka, H., 2011. Tilted wick solar still with flat plate bottom reflector. Desalination 273 (2), 405–413.
Tanaka, H., Iishi, K., 2017. Experimental study of a vertical single-effect diffusion solar still coupled with a tilted wick still. Desalination 402, 19–24.
Thabit, M.S., Hawari, A.H., Ammar, M.H., Zaidi, S., Zaragoza, G., Altaee, A., 2019. Evaluation of forward osmosis as a pretreatment process for multi stage flash seawater desalination. Desalination 461, 22–29.
Velmurugan, V., Deenadayalan, C., Vinod, H., Srithar, K., 2008. Desalination of effluent using fin type solar still. Energy 33 (11), 1719–1727.
Wei, B., Pan, J., Feng, J., Chen, C., Liao, S., Yu, Y., Li, X., 2020. Highly conductive and permselective anion exchange membranes for electrodialysis desalination with series-connected dications appending flexible hydrophobic tails. Desalination 474, 114184.
Zhou, S., Gong, L., Liu, X., Shen, S., 2019. Mathematical modeling and performance analysis for multi-effect evaporation/multi-effect evaporation with thermal vapor compression desalination system. Appl. Therm. Eng. 159, 113759.